The Astronomical Journal, 136:2306–2320, 2008 December doi:10.1088/0004-6256/136/6/2306

THE SLOAN DIGITAL SKY SURVEY-II: PHOTOMETRY AND SUPERNOVA IA LIGHT CURVES FROM THE 2005 DATA

Jon A. Holtzman[1], John Marriner[2], Richard Kessler[3,4], Masao Sako[5,6], Ben Dilday[3,7], Joshua A. Frieman[2,3,8], Donald P. Schneider[9], Bruce Bassett[10,11], Andrew Becker[12], David Cinabro[13], Fritz DeJongh[3], Darren L. Depoy[14], Mamoru Doi[15], Peter M. Garnavich[16], Craig J. Hogan[12], Saurabh Jha[5,17], Kohki Konishi[18], Hubert Lampeitl[19,20], Jennifer L. Marshall[14], David McGinnis[3], Gajus Miknaitis[3], Robert C. Nichol[20], Jose Luis Prieto[14], Adam G. Riess[19,21], Michael W. Richmond[22], Roger Romani[5], Mathew Smith[20], Naohiro Takanashi[15], Kouichi Tokita[15], Kurt van der Heyden[11,23], Naoki Yasuda[18], and Chen Zheng[5]

[1] Department of Astronomy, MSC 4500, New Mexico State University, P.O. Box 30001, Las Cruces, NM 88003, USA; holtz@nmsu.edu
[2] Center for Particle Astrophysics, Fermi National Accelerator Laboratory, P.O. Box 500, Batavia, IL 60510, USA
[3] Kavli Institute for Cosmological Physics, The University of Chicago, 5640 South Ellis Avenue Chicago, IL 60637, USA
[4] Enrico Fermi Institute, University of Chicago, 5640 South Ellis Avenue, Chicago, IL 60637, USA
[5] Kavli Institute for Particle Astrophysics and Cosmology, Stanford University, Stanford, CA 94305-4060, USA
[6] Department of Physics and Astronomy, University of Pennsylvania, 203 South 33rd Street, Philadelphia, PA 19104, USA
[7] Department of Physics, University of Chicago, Chicago, IL 60637, USA
[8] Department of Astronomy and Astrophysics, The University of Chicago, 5640 South Ellis Avenue, Chicago, IL 60637, USA
[9] Department of Astronomy and Astrophysics, The Pennsylvania State University, 525 Davey Laboratory, University Park, PA 16802, USA
[10] Department of Mathematics and Applied Mathematics, University of Cape Town, Rondebosch 7701, South Africa
[11] South African Astronomical Observatory, P.O. Box 9, Observatory 7935, South Africa
[12] Department of Astronomy, University of Washington, Box 351580, Seattle, WA 98195, USA
[13] Department of Physics, Wayne State University, Detroit, MI 48202, USA
[14] Department of Astronomy, Ohio State University, 140 West 18th Avenue, Columbus, OH 43210-1173, USA
[15] Institute of Astronomy, Graduate School of Science, University of Tokyo 2-21-1, Osawa, Mitaka, Tokyo 181-0015, Japan
[16] University of Notre Dame, 225 Nieuwland Science, Notre Dame, IN 46556-5670, USA
[17] Department of Physics and Astronomy, Rutgers University, Piscataway, NJ 08854, USA
[18] Institute for Cosmic Ray Research, University of Tokyo, 5-1-5, Kashiwanoha, Kashiwa, Chiba 277-8582, Japan
[19] Space Telescope Science Institute, 3700 San Martin Drive, Baltimore, MD 21218, USA
[20] Institute of Cosmology and Gravitation, Mercantile House, Hampshire Terrace, University of Portsmouth, Portsmouth PO1 2EG, UK
[21] Department of Physics and Astronomy, Johns Hopkins University, 3400 North Charles Street, Baltimore, MD 21218, USA
[22] Physics Department, Rochester Institute of Technology, 85 Lomb Memorial Drive, Rochester, NY 14623-5603, USA
[23] Department of Astronomy, University of Cape Town, South Africa

Received 2007 October 16; accepted 2008 August 2; published 2008 November 10

ABSTRACT

We present *ugriz* light curves for 146 spectroscopically-confirmed or spectroscopically-probable Type Ia supernovae (SNe) from the 2005 season of the Sloan Digital Sky Survey-II Supernova (SN) survey. The light curves have been constructed using a photometric technique that we call scene modeling, which is described in detail here; the major feature is that SN brightnesses are extracted from a stack of images without spatial resampling or convolution of the image data. This procedure produces accurate photometry along with accurate estimates of the statistical uncertainty, and can be used to derive photometry taken with multiple telescopes. We discuss various tests of this technique that demonstrate its capabilities. We also describe the methodology used for the calibration of the photometry, and present calibrated magnitudes and fluxes for all of the spectroscopic SNe Ia from the 2005 season.

Key words: supernovae: general – techniques: photometric

Online-only material: color figures, tar file (data files), extended figure set

1. INTRODUCTION

In its second phase of operations, the Sloan Digital Sky Survey (SDSS; York et al. 2000) telescope has been used to attack several different scientific problems. One of these is a supernova (SN) survey that ran from 1 September to 30 November for 3 years (2005–2007) and targeted Type Ia supernovae (SNe) in the redshift range $0.05 < z < 0.35$. The project's scientific motivations are (1) to take advantage of the high areal coverage (over 150 deg^2 per night) and moderate sensitivity ($\sim$22 mag) that can be obtained with the large format camera and drift scanning of SDSS to fill in a redshift regime where other surveys have not been efficient in finding SNe, and (2) to take advantage of the well-understood photometric system of SDSS to minimize calibration errors and other systematics. An overview of the observational techniques and expected scientific returns of this program are given in Frieman et al. (2008).

Operationally, two strips (denoted strips 82N and 82S), located along the celestial equator with right ascension between 20 hr and 4 hr, are monitored over a period of 3 months from September through November. These two strips, with a combined width of 2.°5 and an area of approximately 300 deg^2, have been the subject of many previous SDSS imaging scans during the original SDSS survey. The SDSS SN survey alternates between these two strips on successive clear nights. There is a small overlap between the strips (roughly 10% of the area) to insure that no sky coverage is lost. New transients and variable sources are identified by subtracting high signal-to-noise template images, constructed by coadding previous observations of the strip and inspecting the subtracted frames to find new objects. Candidate SNe are identified via a combination

of automated and interactive techniques, and spectroscopically observed using a variety of telescopes to confirm that they are SN and to determine the SN type and redshift. Details of the SNe candidate identification and spectroscopic target selection are given in Sako et al. (2008); details of the spectroscopy and SN typing are given in Zheng et al. (2008). The initial cosmological results from the SDSS-II Supernova Survey are presented in Kessler et al. (2008).

This paper presents the techniques used to measure the brightnesses of the SNe for final analysis. We discuss the photometric calibration, photometric techniques, and expected errors in the resulting photometry, and present the resulting light curves for spectroscopically-confirmed, and likely type Ia, SNe from the first season (2005) of the SDSS-II Supernova Survey.

2. DATA AND DATA REDUCTION

2.1. SDSS Imaging

The imaging data are taken using the SDSS imaging camera (Gunn et al. 1998) on the SDSS 2.5 m telescope (Gunn et al. 2006) at Apache Point Observatory (APO). This camera uses 30 imaging CCDs arranged in six columns; each column has a detector for each of the five SDSS filter bandpasses, *ugriz* (Fukugita et al. 1996). Additional detectors are used to assist with the astrometric calibration (Pier et al. 2003) of the science frames. The camera runs in a drift scanning mode such that each column is exposed for 54 s per filter, with a slight time lag between successive filters. Operation of the camera for the SDSS-II SN survey is identical to routine operation for the original survey (see Stoughton et al. 2002 and Adelman-McCarthy et al. 2008 for details of the survey operation and data releases).

The imaging data are processed through the standard SDSS processing pipeline, which uses the program PHOTO (R. Lupton et al. 2008, in preparation) to remove instrumental signatures, flag bad pixels, determine a point-spread function (PSF), and create an object catalog with instrumental brightnesses. As output, PHOTO produces corrected frames, which have instrumental signatures removed and astrometric information in their headers, and mask frames that flag problematic pixels. Each column of a strip in the sky is divided into a series of adjacent fields (2048 × 1489 pixels, or roughly 800 by 600 arcsec^2), for output, with a small amount of overlap between fields.

For the purpose of identifying SNe during the survey, template images from previous imaging scans are subtracted from the images from each SN run. For the 2005 observing season, we used data from pre-2004 SDSS runs to create a co-added template. These co-added templates were constructed from a combination of between four and nine photometric runs with good seeing. Before subtracting the template, a smearing kernel is applied to the template to match its PSF to the PSF of the SN frame, and the template frame is astrometrically registered to the SN frame. Details of the astrometric and PSF matching are given in an appendix in Sako et al. (2008). We refer to the resulting subtracted frames as the `Framesub` data. These data are used for identification of candidate SNe, and for initial photometry that is used for target selection for spectroscopic followup; our final photometry, as discussed below, is more accurate, but is not used for target selection.

2.2. Other Imaging

Additional imaging of SDSS-II SN candidates was obtained from several other telescopes: primarily, the 2.4 m MDM telescope on Kitt Peak, the 88 inch UH telescope on Mauna Kea, and the ARC 3.5 m and NMSU (New Mexico State University) 1 m telescopes at APO. The main goals of these observations were to increase light-curve coverage during periods of poor weather that limited the temporal coverage of the SDSS 2.5 m data, to allow deeper observations for more distant SN and/or at later epochs than can be obtained with the fixed 54 s integration time of the 2.5 m telescope, and to measure the light curves of SNe discovered late in the survey season into the month following the completion of the SDSS imaging. During the 2005 campaign, the APO weather was generally quite good, so these additional observations were not as critical as they might have been in poor weather.

On all of the non-SDSS telescopes, filter sets approximating the SDSS filter set were used, but there are still small but significant differences between the response functions. This is a serious issue for the SN program, since we hope to reduce the systematic errors in the photometry to ∼0.01 mag. In Section 4.1.2, we discuss the techniques used to extract the SN photometry from these other telescopes and the issues involved with using this photometry in a joint analysis with the 2.5 m data.

3. PHOTOMETRIC CALIBRATION

The SDSS-II SNe runs are taken on all fall nights during which the telescope can be operated, except for five nights around full moon. Much of the data are taken under nonphotometric conditions. However, all of the data on strips 82N and 82S taken as part of the standard SDSS-I survey (before 2004) were taken under photometric conditions, with simultaneous monitoring of atmospheric transmission using the SDSS Photometric Telescope (PT). As a result, the standard SDSS-I imaging provides multiple photometric measurements of all stars along these strips. The details of the photometric calibration of the SDSS images are discussed in Hogg et al. (2001), Smith et al. (2002), Ivezic et al. (2004), Tucker et al. (2006), and on the SDSS Web pages.[24]

Ivezic et al. (2007) had taken the repeat observations along the equatorial strips and constructed a master catalog of standard stars in the SDSS system using these measurements. Variable stars are flagged by comparing the multiple measurements, and final median magnitudes for all nonvariables with good signal-to-noise were compiled into the master catalog. A variety of tests with these measurements suggest that the catalog magnitudes are accurate to within ∼0.01 mag.

We use the Ivezic et al. (2007) catalog to calibrate the SNe frames. The details of which stars are used vary for the different photometric techniques, as discussed below, but, in general, brightness measurements of a set of stars are made around each SN candidate, and these measurements are compared with the catalog to determine photometric zero points for measurements of that candidate. Along with the derived zero points, the scatter of the observed star brightnesses relative to the catalog brightnesses is computed to determine how well single zero points match the frames; with the drift scanning that is used for the survey, stars at different right ascensions are observed over

[24] http://www.sdss.org

different time intervals, so the zero point can vary as a function of the row position on the frames.

The number of calibration stars varies along the SDSS SN strip, largely due to the variation in Galactic latitude. The number of calibration stars around each SN varies from a few to several hundreds. However, in many cases, a large fraction of the calibration stars do not have *u*-band magnitudes in the calibration catalog, which limits our ability to extract *u*-band measurements for some objects.

Finally, the Ivezic et al. (2007) catalog does not quite extend to the western end of the SN strip, in the first 10° of the SN strip, because only a smaller number of SDSS runs covered this area. In this region, we have constructed an analogous calibration catalog, but since it is based on fewer observations, the uncertainties in the calibration are a bit higher in this region.

3.1. Absolute Flux Calibration

The Ivezic et al. (2007) catalog is calibrated to the native SDSS survey photometric system. While this system was originally intended to be an AB system (Oke 1974; Fukugita et al. 1996), it was realized that the inclusion of the effects of atmospheric transmission makes it differ slightly (at about a 4% level) from an AB system in the *u*-band; subsequent observations of calibrated targets suggest that, at the 1%–2% level, the survey photometry may differ from that of a true AB system in the other bandpasses as well.

Various efforts have been made to understand the absolute calibration of the SDSS system. Here, we calibrate to the *Hubble Space Telescope* (*HST*) white dwarf system (Bohlin 2007). Bohlin (2000) and Bohlin et al. (2001) presented calibrated spectra for several white dwarfs and solar analog stars in this system. Unfortunately, all of these stars are too bright to be directly observed using the SDSS 2.5 m telescope, and, in any case, none of them are in the region of the sky where multiple SDSS observations have been made. However, several of these stars have been observed numerous times by the SDSS PT, which is normally used to transfer photometric zero points to data taken with the SDSS 2.5 m telescope. While SDSS-like filters are used on the PT, the system response functions are not exactly the same between the two telescopes, so color terms have been determined to allow for the transformation of magnitudes observed on the PT to the SDSS system (which is defined as the system of the 2.5 m telescope). These color terms have been defined over a relatively narrow range of color, corresponding to F- and G-type stars. As a result, while the color terms do not strictly apply to the white dwarf standards, the solar analog standards nicely fall within the color range for which the color terms have been determined.

There are three solar analogs for which ten or more PT observations have been made: P330E, P177D, and P041C. The observed PT measurements were transformed to the SDSS system using the standard survey color terms (Tucker et al. 2006). These SDSS measurements were then compared with synthetic AB magnitudes calculated using the calibrated spectral energy distributions (SEDs) of the stars and the SDSS system response curves (from the SDSS Web site[24]). Differences between the synthetic and observed magnitudes are then interpreted to be the deviation of the SDSS system from a true AB system. The average magnitude offsets (AB-SDSS) for the three stars are determined to be −0.037, 0.024, 0.005, 0.018, and 0.016 mag for *ugriz*. Table 1 summarizes the observed and synthetic magnitudes for the solar analogs, and the average offsets; the offsets are defined such that they need to be added to the SDSS magnitudes to bring them onto an AB system.

Table 1
Observed and Synthetic Measurements of Solar Analogs

Star	*u*	*g*	*r*	*i*	*z*
Observed mags (transformed to SDSS)					
P330E	14.548	13.280	12.841	12.701	12.674
P177D	15.118	13.745	13.300	13.158	13.125
P041C	13.573	12.260	11.844	11.719	11.703
Synthetic mags					
P330E	14.506	13.303	12.839	12.708	12.675
P177D	15.085	13.776	13.307	13.178	13.142
P041C	13.537	12.279	11.852	11.746	11.732
Differences ($m_{syn} - m_{obs}$)					
Δm	−0.037	0.024	0.005	0.018	0.016
rms Δm	0.005	0.006	0.005	0.010	0.014

We adopt these offsets for our SN photometry, since accurate absolute calibration is important for cosmological analysis of the SNe data. Note that these offsets rest on the assumptions of (1) correct SEDs for the solar analogs, (2) correct observations of the solar analogs, (3) correct transformations of the observations to the SDSS system, and (4) correct knowledge of the SDSS system response.

We recognize that further refinements to the absolute calibration may be available in the future. We note that several other efforts have been made to understand the relation of the SDSS system to an AB system (see the SDSS Web site)[24] that yields results similar, but not identical, to those adopted here. Differences in these analyses at the 1%–2% level are consistent with our calibration error estimate of about 1%.

Because of potential refinements to the absolute flux calibration, we present two versions of SN photometry for the data associated with this paper: magnitudes on the native SDSS system (no AB correction) and fluxes that have been determined using the AB corrections discussed above.

4. PHOTOMETRY METHODS

After the images are taken, initial, rapid photometry is required to identify candidates for spectroscopic followup (Sako et al. 2008). This quick photometry, which we call "search photometry," measures SN brightnesses using a modified DOPHOT (Schechter et al. 1993) technique on the pipeline template-subtracted frames. Each observation in each filter is processed independently. Objects are not required to be present at a common position in all filters and epochs and may be found in some filters but not others. The initial search photometry meets the goal of SN detection and measurement (generally much better than the 10% accuracy goal), but it does not provide the most accurate treatment of the data possible.

For the final photometry, we investigated three different techniques. The first, which we call "forced photometry," also works on the template-subtracted frames, but the photometry reduction forces the position of the SN to be the same on all frames, where the forced position is determined from the average of the search photometry positions in frames where the SN is within 1 mag of its peak observed brightness. Forced photometry is used during the SN search to obtain photometry on SN candidates for epochs and filters in which an object was not detected by the initial photometry. For both search and forced photometry, the astrometric and photometric scalings of each frame are adopted from the `Framesub` software.

Two independent techniques that recompute the astrometric and photometric scalings, as well as provide independent photometry on the SNe, were also developed. One, which we call "cross-convolution" photometry, measures stellar positions and intensities on search and template frames, and determines an astrometric solution and a photometric scaling. The template frame is convolved with the PSF of the search frame and the search frame is convolved with the PSF of the template frame; this avoids the requirement of parameterizing the PSF as is done in frame subtraction pipeline. The convolved template frame is subtracted from the convolved search frame, and the magnitudes are determined by weighted PSF photometry on the difference, again requiring the same position for the SN in all frames. The cross-convolution photometry uses PSFs as measured by the PHOTO pipeline.

Finally, we developed a technique that does not use template-subtracted frames, but instead fits all of the individual reduced frames with a model of the galaxy background and SN; we call this technique "scene-modeling" photometry. Ultimately, we chose to use "scene modeling" as the final photometry because of its theoretical advantages, its superior ability to provide "smooth" SN light curves, and accurate error estimates from first principles; no convolution or resampling of any image data is involved. Details of the technique are given in the next section. The other approaches are mentioned here to demonstrate that we made significant effort to determine the optimal photometry for the SN light-curve analysis.

4.1. Scene Modeling Photometry

The main idea behind our scene modeling technique is to perform photometry on individual calibrated images without degrading the PSF and without any spatial resampling that leads to correlated noise between pixels. All of the frames are simultaneously fit with a model of the galaxy background plus SN. This is statistically optimal in that the model produces a prediction for each observed pixel that can be compared to the observation and its error; propagation of pixel level errors to fitted quantities is made in a precise and rigorous fashion.

The basic concept is similar to the technique used by the Supernova Legacy Survey (SNLS; Astier et al. 2006), but developed independently, and includes a new key feature, namely no spatial resampling. The photometry described in Astier et al. (2006) is accomplished by modeling each image as the sum of a time-independent galaxy background plus a time-dependent SN and convolving the model with a separate PSF for each image; however, all images are resampled to a common pixel grid before doing the fit. This leads to correlated errors between adjacent pixels, which, as described by Astier et al., lead to underestimated parameter uncertainties, including the uncertainty on the SN flux measurements. Astier et al. estimated that the variances returned from the fit are 25% too small as a result of the pixel correlations. Because of this, they adopted empirical uncertainties derived from multiple observations on a given night. They found that the typical variances as derived from repeat observations are about 50% larger than those predicted from the fits. Our implementation does not involve any spatial resampling of the images, so there are no correlated errors that can cause derived errors to be underestimated. The tests described in Section 5 demonstrate that our error estimates are accurate.

We note that our technique provides the largest benefits when the pre-SNe template images are of comparable (or lower) signal-to-noise to the SNe images and/or the seeing in template images is worse than that of the images with the SNe. If high signal-to-noise and good seeing template images are available, these can be resampled and degraded to the pointing and resolution of the SNe frames without introducing too much correlated noise (because in this case, the SN frame, rather than the template, dominates the noise).

Aside from the modeling technique, our technique is customized for the SDSS survey to take advantage of the pre-existing photometric catalog of stars in the SN fields.

We model each image as the sum of a set of stars, a galaxy, a SN, and background. The galaxy is modeled as a grid of squares of constant surface brightness. The stars and SN are modeled as point sources, with magnitudes that are time-independent and time-dependent, respectively. A separate PSF is determined for each image, and each image is matched to the model convolved with the image's PSF. A set of stars are used to determine the relative astrometric and photometric transformations between the frames, and the stars and SNe are required to have the same relative positions in every frame.

The algorithm proceeds as follows. A set of calibration stars are extracted from our calibration star list around the position of each SN. For each SDSS observation of each SN, a 2048×1024 pixel image subsection ($\sim 800 \times 400$ arcsec^2) is cut out of the PHOTO-corrected frames in each filter, with the SN centered in rows in the cutout (adjoining fields are pasted together if necessary). Hereafter, we refer to the image subsections as frames. Since the SDSS data are taken in a drift-scanning mode, the mean time of observation differs by about 27 s from bottom to top of these image subsections. The calibration stars are sorted by brightness. Since the calibration stars only include nonvariable stars and do not extend to the faintest stars in the frame, a star finding algorithm is used on a single g-band frame to obtain a more complete star list. Using this star list, any object from the calibration star catalog that has a nearby object is excluded to ensure that the final calibration list contains only isolated stars.

For each frame, a slowly varying background model is derived by determining a sky value in 25 (a 5×5 grid) subsections within the image. The sky level per pixel in each subregion is measured using an estimate of the modal value (Stetson 1987) in the region; the final sky level is remeasured after rejecting values 5σ larger than the initial estimate (to further minimize effects of stars). A quadratic fit is done to these 25 values to provide a model of the sky background. The root mean square (rms) of the 25 independent measurements is compared with the standard deviation in the central region; if the variation across the entire frame is larger than expected from the individual variances, the frame is flagged as having a potentially uncertain sky level; the source of the variation in such frames can arise from rapid changes in atmospheric conditions, and, in some cases, from the presence of a very bright star in or near the image subsection. Only a small fraction of all of our images show this behavior.

On each frame, stars are identified using the DAOPHOT (Stetson 1987) FIND algorithm for potential use in determining the PSF; we use more than just calibration stars for this purpose since even variable stars are useful for the determination of the PSF. This star list is filtered to remove all objects with nearby neighbors, and any object with shape parameters that significantly deviate from those measured for the bulk of the stars. On each frame, aperture photometry measurements are made for the stars in the filtered list. A position-independent PSF is created for the image frame using all stars within 3 mag

of the brightest star in the field. A constant PSF gives an adequate representation (in most cases) over the moderately small image subsection that we use. In any case, there are generally too few stars to derive an accurate PSF model with spatial variation. The PSF representation is made using the PSF characterization of DAOPHOT (Stetson 1987): a Gaussian integrated over pixels is fit to the brightest PSF star, and the residuals from this Gaussian are stored in a lookup table at 0.5 pixel spacing. The removal of an underlying Gaussian minimizes the effect of interpolation errors in the lookup table. For any additional PSF star, the integrated Gaussian from the brightest star is fit to each star individually, and the residuals are interpolated and added to the lookup table to reduce noise. The PSF is assumed to be zero beyond a specified PSF radius.

We then proceed to fit a model to the observed data. At each pixel with coordinates (x, y) and in a given filter, the model for the flux is given by

$$M(x, y) = \mathrm{sky}(x, y) + S\left(\sum_{\mathrm{stars}} I_{\mathrm{star}}\mathrm{PSF}(x - x_{\mathrm{star}}, y - y_{\mathrm{star}}) + I_{\mathrm{SN}}\mathrm{PSF}(x - x_{\mathrm{SN}}, y - y_{\mathrm{SN}}) + \sum_{x_g, y_g} \mathcal{G}(x_g, y_g)\mathrm{PSF}(x - x_g, y - y_g)\right), \quad (1)$$

where x and y are the horizontal and vertical pixel indices, respectively, $M(x, y)$ is the total model intensity (DN) at each pixel, I_{star} is the known total calibrated brightness of each star, I_{SN} is the unknown total calibrated SN intensity, $\mathrm{PSF}(\Delta X, \Delta Y)$ is the measured fraction of light from a star as a function of the distance of each pixel from the stellar position, $\mathcal{G}(x_g, y_g)$ represents the unknown grid of galaxy intensities, and $\mathrm{sky}(x, y)$ is the measured background value at each pixel. S is the unknown frame scaling factor that converts the calibrated fluxes to DN on each individual frame. The positions $(x_{\mathrm{star}}, y_{\mathrm{star}})$ and $(x_{\mathrm{SN}}, y_{\mathrm{SN}})$ are the pixel coordinates of the stars and SNe, respectively, which are derived from their celestial positions and an astrometric solution for each frame.

The fits are weighted by the expected errors from photon statistics and readout noise, using the gain (G; the number of DN per detected photons) values for each camera column and each filter as given in the SDSS `fpAtlas` files. We adopted $\sigma_{rn} = 5$ electrons for the readout noise; technically, the readout noise varies from chip to chip, but a single typical value was adopted since it is a negligible noise source. Specifically, we minimize

$$\chi^2 = \sum_{xy} \frac{(O(x, y) - M(x, y))^2}{\left(M(x, y)/G + \left(\frac{\sigma_{rn}^2}{G^2}\right)\right)}, \quad (2)$$

where $O(x, y)$ is the observed value at each pixel. Operationally, we limit the model to include stellar (and SN) flux out to a PSF radius of 5 arcsec from the center of each object. Due to lower signal-to-noise in the outer regions of the PSF, only pixels within a specified fitting radius (which is taken as 3 arcsec or the measured FWHM of the PSF, whichever is larger) are used in adjusting the fit parameters, but the contribution of objects out to 5 arcsec is included in the model.

Since the model is nonlinear in the fit parameters, the solution is iterated from a starting guess. Adjustments to the initial parameters are computed using the full Hessian matrix, using a Levenberg-Marquardt scheme. If the fit has abnormally large χ^2 after several iterations, the weight of pixels with large χ^2 ($> 2.5\sigma$) is decreased; this attempts to prevent bad pixels from corrupting the fit quality. The fit is judged to converge when all of the point source intensities do not significantly change in an iteration.

The first step in solving for the model parameters is to determine accurate stellar positions for the stars on the calibration list. The initial positions from the calibration catalog are average positions from the pre-SN template catalog. However, since the SDSS template images of the SDSS SN survey area go back to 2001, proper motions are not negligible for some stars, and allowing for proper motions significantly improves the quality of the model fits to the data. Our first fit solves for stellar positions and proper motions using a subset of the SDSS r-band images. For this fit, we take the initial epoch and subsequent epochs separated by 60 or more days from the previous epoch. To maximize the baseline for proper motion determination, we use all SDSS data taken from the beginning of the SDSS survey (2001) until the end of the SDSS SN survey (2007); this typically gives us 10–20 images to fit. The stack of image subsections is simultaneously fit for stellar positions (at epoch 2000), proper motions, an astrometric solution for each frame, and photometric frame scalings between the frames. We arbitrarily adopt the SDSS astrometric solution of the first frame in the list as the absolute reference frame, since all we really care about is accurate relative astrometry between the frames. This process yields us a list of stars with accurate relative positions on the sky, proper motions, and calibrated brightnesses. Since the fit only includes stars, the proper motions are not absolute, but are only relative (in the fit, we lock the proper motion of the first star to be zero); after the fit, we normalize them so that the mean proper motion of all of the stars is zero (but we allow for a proper motion of the reference frame in the galaxy fit; see below).

For the astrometric model, we adopt the distortion coefficients measured by the SDSS photometric pipeline, but solve for a full linear astrometric solution (six parameters) within each of our subframes. For any frames where only three calibration reference stars are available, we constrain the astrometric solution to fit only four parameters for scale, rotation, and offset.

Given measured stellar positions, our second series of fits solves for the frame scale factors, S_{frame}, and the astrometric parameters for each frame. These can be determined for each frame independently, since all of the stellar parameters (positions, proper motions, and intensities) are held fixed in the fit. Only frame parameters (which are independent from frame to frame) are solved for; in these fits, there are seven parameters (six linear astrometric parameters plus 1 photometric frame scaling). A single photometric frame scaling value for our subsections requires stable transparency over a time interval of $\sim$81 s and over a spatial scale of $\sim$800 arcsec. Based on the residuals of stars across the field, we have found, to no surprise, that the assumption of a single photometric frame scale-value becomes less accurate under cloudier conditions. As a result, we flag all frames where the photometric scaling is less than half the expected scaling for photometric weather (allowing for differences in airmass).

To identify frames that may have other problems, and to assess the quality of the astrometric/photometric solution, a final fit iteration is performed after the frame solution is determined; in this final iteration, we lock the frame parameters and stellar positions and fit for the individual stellar brightnesses. These recovered brightnesses are compared with the known brightnesses from the calibration star catalog. A subset of the

best-measured stars is selected so that it contains at least five stars (three in the u-band). The mean magnitude difference, rms, and χ^2 for this set of stars are computed using the fit brightnesses and error estimates; for the χ^2 calculation, an error term is included for the uncertainties in the calibration magnitude of each star. The reduced χ^2 for the frame is recorded, and all frames with atypically large χ^2 are flagged. Finally, we estimate a "frame error" term by determining what additional error needs to be added (in quadrature) to bring the reduced χ^2 down to unity; this term is generally less than 0.01 mag, and is plausibly associated with errors that result from inaccuracies in the PSF model.

Figure 1 shows the difference of the recovered stellar magnitudes and the calibration magnitude for all of the calibration stars for all of the 2005 confirmed type Ia SNe as a function of stellar brightness and color. These plots demonstrate that we accurately recover the brightnesses of the calibration stars with our PSF fitting, and display the typical photometric errors in our exposures as a function of stellar magnitude.

The derivation of astrometric parameters and photometric scaling factors for each of the SNe frames discussed so far is similar to what is done for most SNe surveys, although the inclusion of proper motions may not be typical (or needed, when the time baseline is short). We also have attempted to do a careful accounting of errors.

In the third, and final, fitting stage, we extract a small 128×128 ($\sim 50 \times 50$ arcsec^2) image subsection around the position of the SN in every frame. Using the derived-frame photometric scalings and astrometry, we simultaneously fit the entire stack of images (all epochs and all filters) to solve for a temporally constant galaxy plus a temporally variable SN. Frames that have been flagged as potentially unreliable in any of the previous steps are not allowed to influence the galaxy model, but are still included for a determination of the SN brightness (as described below, the flag is carried along for the final output). We obtain the estimated SN peak intensity date from the search photometry, and force all observations that were more than 90 days before peak to have zero SN flux. For a typical SN, the image stack contains several hundred images: 10–20 pre-SN images and 10–20 SN images in each of five filters. A single SN position is fit to the entire stack. The galaxy is modeled as a grid of squares of constant surface brightness; we use a 15 by 15 grid of 0.6 by 0.6 arcsec^2, with independent brightnesses in each of the five filters at each location. The model galaxy size of 9 by 9 arcsec^2 around the position of the SN may not model the entire galaxy, but models a sufficient amount to determine the galaxy contribution at the position of the SN, even under the worst-seeing conditions. The galaxy model is interpolated to the pixels on each frame separately; the choice of the model grid spacing is not critical. Given the typical SDSS seeing of $\sim$1.2 arcsec, it is clear that information at the 0.6 arcsec scale is limited, and, in fact, the recovered galaxy maps often do not show realistic structure at this spatial scale. However, when the recovered maps are smoothed to the typical seeing, they match the observed galaxy well, and the relatively fine sampling allows us to match regions with steep intensity gradients. We have tried using both coarser and finer samplings for the galaxy model, and find that the SN photometry is relatively insensitive to sampling changes. The SN is allowed to have a separate brightness in each frame, but is required to have a common position in *all* frames; the position is iteratively determined by the fit using all of the available data. The total number of fit parameters in the final fit is

$$N_{\rm fit} = (15 \times 15)N_{\rm filt} + N_{\rm epoch} * N_{\rm filt} + 4, \quad (3)$$

where $N_{\rm filt}$ is the number of filters (usually five, but sometimes four if there are an insufficient number of u-band calibration stars) and $N_{\rm epoch}$ is the number of epochs observed later than 90 days before the estimated SN peak. The final four parameters are for the celestial position (α, δ) of the SN and the mean proper motion of all of the calibrating stars in the field; it is the galaxy light that constrains the mean proper motion of the calibration stars.[25]

Output from the final fit includes SN brightnesses for each frame along with error estimates from the least-squares fit. Since the noise model is derived from photon statistics and readout noise, but does not include terms from an imperfect PSF or inaccuracies in the determination of the frame photometric zero points or sky model, the least-squares errors may be underestimated, especially for the brightest points where statistical errors are small. In an attempt to provide realistic error estimates for all points, we take the errors from the fit and add in the individual "frame errors," the derivation of which was previously described. Since these are derived from observations of relatively bright stars, they are expected to account for errors in PSF modeling and frame scaling.

Two other sources of error are also considered: error arising from inaccuracies in the sky estimate and error from inaccuracies in the galaxy model at the location of the SNe. The former gives a systematic error over the pixels covered by an SN at any individual epoch, but is likely to be a random error source for different SN epochs. The galaxy model error gives systematic errors that are similar (not identical, because of seeing variation) for all epochs of a given SN. We estimate the sky error based on the variation of the sky level from different subsections of the frame (although in cases where there is real structure in the sky background, this might overestimate the sky error). The galaxy error is calculated from the least squares fit, and includes correlated errors that exist between adjacent locations in the galaxy model since this model is sampled finer than the PSF; this estimate of the galaxy error may be an underestimate since it does not account for errors that would result from systematic errors in the astrometric solution of the frames. Since the portion of the galaxy that contributes flux at the location of the SN depends on the seeing, the galaxy error can vary from frame to frame; for output, we calculate a typical galaxy error that arises for a seeing of 1.2 arcsec. The estimated errors from inaccuracies in sky and galaxy subtraction are output, along with the SN brightness and its random error. Clearly, the importance of the sky and galaxy subtraction errors is larger when the SN brightness is comparable to or fainter than the sky or galaxy. In general, errors in the sky background dominate those in the galaxy model.

We have created images of the frame with the model subtracted, and inspection of these provides qualitative confirmation of the model (see below for some quantitative tests).

Figures 2 and 3 show an example of the procedure applied to one measurement of one of our SNe. Figure 2 demonstrates the initial astrometric and photometric solution that is determined for each frame individually. The left image shows the image subsections that are used; circles show the calibration reference stars and the square shows the SN. The right image shows the same frame after the best-fit model has been subtracted. Figure 3 shows the region around the SN that is used to

[25] For hostless SNe, the mean proper motion would be unconstrained, but for such objects, there is no pre-SN galaxy background that needs to be accounted for, and proper motions are negligible over the decay time of the SN.

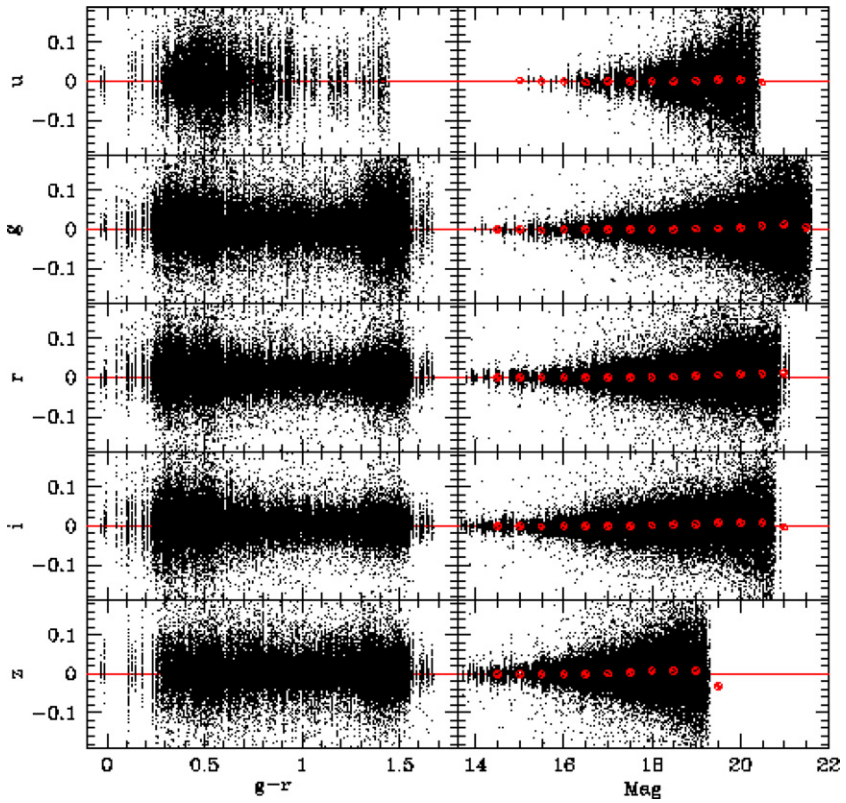

Figure 1. Difference between recovered stellar magnitudes and the calibration magnitudes as a function of stellar color (left panel) and stellar magnitude (right panel). This demonstrates the accuracy of our PSF photometry and also indicates typical errors as a function of stellar brightness.

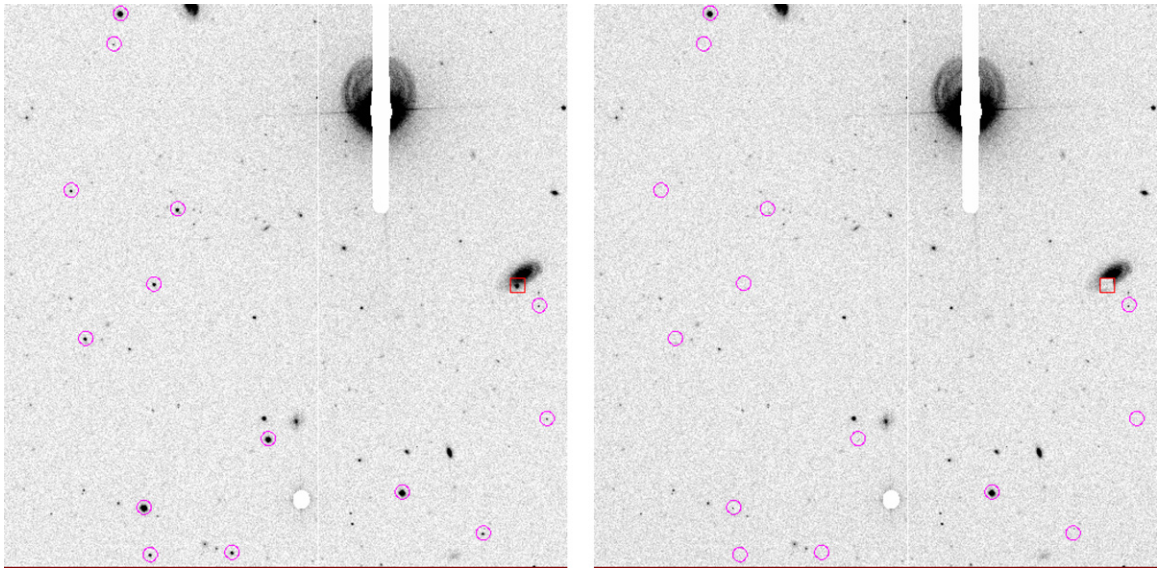

Figure 2. An example of an image subsection used to solve for frame parameters in the second fitting stage, that is, the astrometric solution and photometric scale factor. The stars with circles are the calibration stars used to determine the solution. The left panel shows the image before the model is subtracted, with circles around the calibration stars and a box around the SN; the right panel shows the image after model subtraction.

simultaneously solve for galaxy background, SN position, and SN brightness at each epoch; in this stage, an entire stack of these images is fit simultaneously.

We note that the scene modeling technique does not require perfect spatial overlap between all of the images, as long as there are some stars in common in all of the frames to allow the determination of accurate relative astrometry. For SN that lie in the overlap between strips 82N and 82S, there may be few, if any, reference stars in common between the northern and southern strips. In these cases, the entire dataset is still fit simultaneously. However, the final iteration allows for a global shift between all of the frames in one strip to those in the other strip; similarly, the two strips are allowed to have different mean stellar proper motions. It is the galaxy itself that provides the information to determine the global shift and proper motion difference between the two strips.

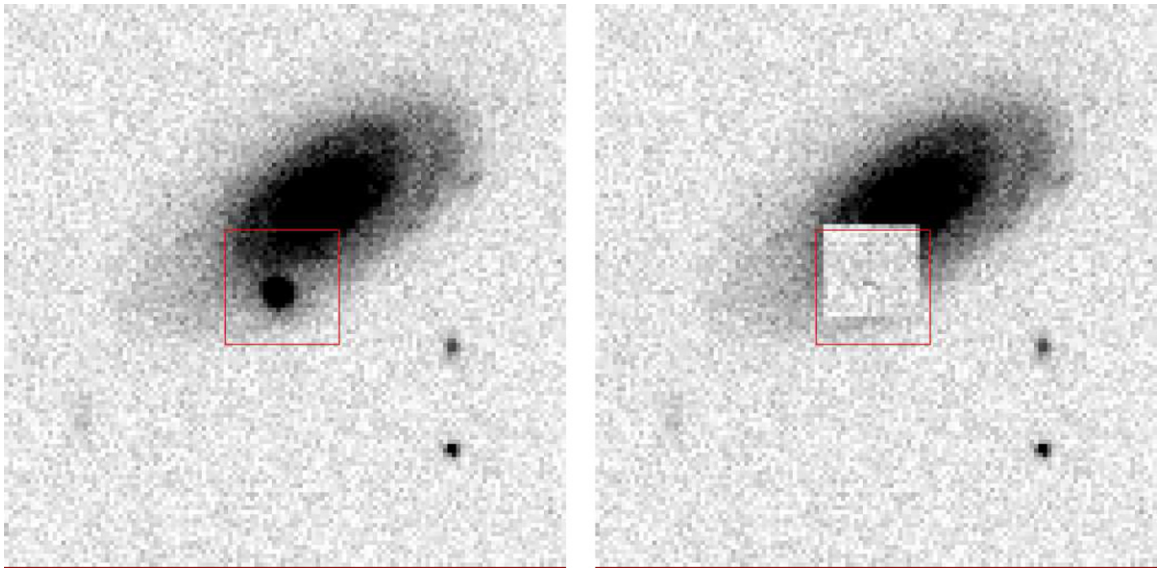

Figure 3. An example of an image subsection used to solve for galaxy background and SN brightness. In this third fitting stage, an entire stack of images, including those with and without the SNe present, is fit simultaneously. The left panel shows the image before the model is subtracted, with a box around the SN; the right panel shows the image after model subtraction.

(A color version of this figure is available in the online journal.)

4.1.1. Data Flags

For each SN measurement, we set a flag to allow for points of potentially poorer quality to be recognized. The value of the flag is a bitwise combination of multiple criteria.

1—Sky brightnesses more than twice median sky brightness from the entire stack of images in this filter, that is, moon or clouds;

2—FWHM of stellar images larger than 2 arcsec, that is, poor seeing;

4—photometric scale factor less than 0.5, that is, moderately cloudy conditions;

8—atypical sky variation: ratio of sky variation between image subsections to sky variation within a subsection significantly larger than the median of entire stack in this filter (can arise under cloudy conditions);

16—large sky variation: large ratio of sky variation between image subsections to sky variation within a subsection (indicator of clouds, but can also arise from the presence of a bright star nearby);

32—derived SN brightness fainter than underlying galaxy brightness (measured using the PSF of the frame);

64—fewer than five calibration stars on frame;

128—rms photometry of calibration stars atypically large;

256—fit exceeded the maximum number of iterations, or fit quality (from individual frame χ^2) poorer than typical;

512—no calibration stars;

1024—photometric scale factor so low, rms photometry of calibration stars so high, variation in sky brightness so high, frame fit quality so poor, or global fit quality so poor, to strongly suggest that data should not be used, that is, *bad data*.

The highest quality points have a flag value of 0. Flag bits of 1, 2, 3, 8, 16, 64, and 128 are determined from the individual frame fits before the global-galaxy–SN solution is determined. Frames with any of these flags set are not used to influence the galaxy model in the final fit, with the exception of flag = 16. This flag can be set because of background light from a nearby very bright star. In this case, the problem persists at all epochs, and a result can be obtained only if these frames are used.

Most points with $0 < flag < 1024$ appear to be of good quality, judging from how well they fit on the light curves. Bit 6 (32) flags points where the SN is fainter than the underlying galaxy, and, as a result, applies to many points for objects buried within bright hosts and to many late time points. These are the points that are most sensitive to the accuracy of the galaxy model, and are most subject to the possibility of systematic error.

Observations with the 1024 bit set, that is, $flag > 1024$, are generally unusable, and should not be trusted. For applications where only the cleanest (potentially highest accuracy) data are desired, even at the expense of throwing away many apparently good points, one might choose to only use points with $flag = 0$. The SDSS cosmology analysis (Kessler et al. 2008) uses essentially all points with $flag < 1024$.

4.1.2. Including Non-2.5 m Data in Scene Modeling

An important feature of the scene modeling technique is that the model is independent of telescope characteristics such as pixel size and registration relative to the model. It is, therefore, straightforward to combine data from different telescopes in the same fit. The same catalog stars can be used to calibrate the response of all the telescopes.

In general, each telescope will have its own unique set of filter response curves. As a result, relative photometry of objects with different SEDs will differ from telescope to telescope. If the differences in filter response from telescope to telescope are small, then the differences can be parameterized by use of a linear color term. For the non-2.5 m data, when deriving the photometric scaling for each frame from the calibration stars, we allow for a color term to be fit as well as a photometric zero point. Since we expect the color term to be constant in time, at least over an observing season, we adopt an average color term

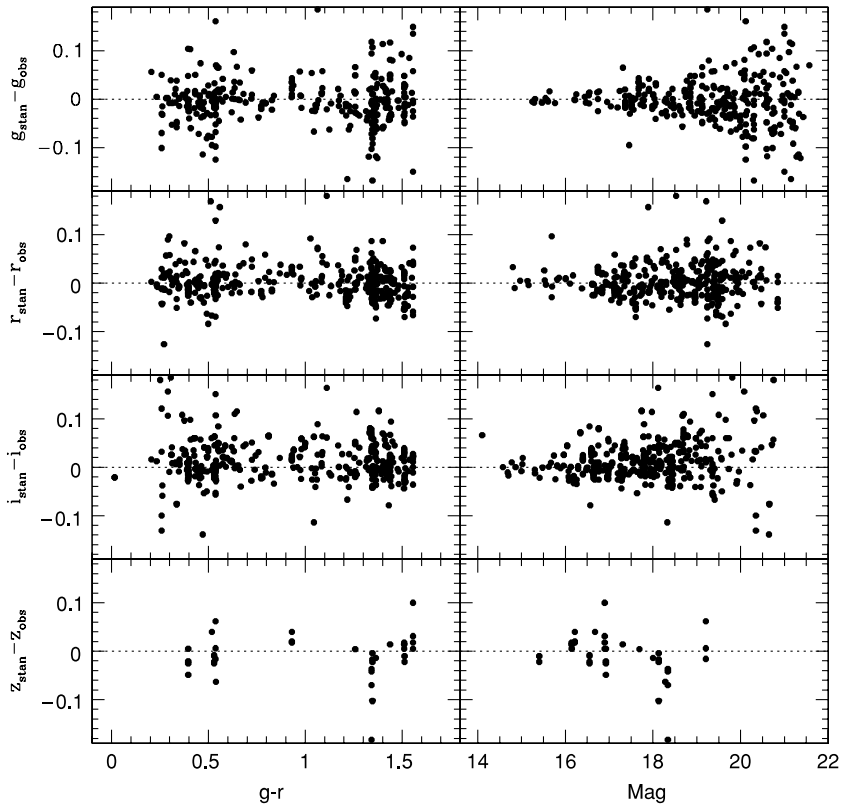

Figure 4. Difference between recovered and calibration photometry for calibration stars in the MDM frames, using the color terms presented in the text.

from the photometric solutions for all frames in a given filter using all of the SNe observed in the 2005 season; this allows for a large range of stellar colors to be sampled.

For the 2005 season, photometry of the SDSS SNe was obtained with several other telescopes; in most cases, only 4-color (*griz*) observations were obtained. Each individual frame was fit to the calibration star list derived from the SDSS frames exactly as above, except that a color term was included when fitting the instrumental brightnesses to the catalog brightnesses. For each telescope, color terms of the form

$$g = g_{\rm obs} + t_g(g - r) \tag{4}$$

$$r = r_{\rm obs} + t_r(r - i) \tag{5}$$

$$i = i_{\rm obs} + t_i(r - i) \tag{6}$$

$$z = z_{\rm obs} + t_z(i - z) \tag{7}$$

were determined, requiring time-independent transformation coefficients over the length of the observing season.

Figure 4 shows an example of the photometric calibration results for all of the stars on MDM 2.4 m frames from the 2005 season after the derived color terms have been removed; this plot is equivalent to Figure 1 for the SDSS frames. The adopted color equations (that are applied for this plot) are

$$g = g_{\rm MDM} - 0.1(g - r) \tag{8}$$

$$r = r_{\rm MDM} - 0.05(r - i) \tag{9}$$

$$i = i_{\rm MDM} + 0.08(r - i) \tag{10}$$

$$z = z_{\rm MDM}. \tag{11}$$

Similar relations have been derived for the other telescopes used during the survey.

The differing filter responses also affect the underlying galaxy background. To account for this, we apply the stellar color term to the underlying galaxy model as well. The accuracy of the application of a color term depends on the degree to which the SED of the object to which the color term is applied (the galaxy, in this case) is similar to the SED of the objects (stars, in this case) used to derive the color term. While SEDs of galaxies are not identical to those of stars, at the moderate redshifts considered here, they are not dramatically different. Combined with the fact that the color terms are relatively small (since SDSS-like filters were used on all of the non-2.5 m telescope), we feel confident that the application of the stellar color terms to the galaxy background model is adequate.

For the final SN photometry, the non-2.5 m frames can be included in the final photometry iteration described above. However, to insure that any issues with the photometric transformation for the non-2.5 m data do not deteriorate the quality of the SDSS 2.5 m photometry, we do not allow the non-2.5 m data to contribute to the solution of the galaxy model itself; only 2.5 m data are used to constrain this model, and the inclusion (or lack thereof) of non-2.5 m data has no effect on the 2.5 m photometry.

Interpreting the SN photometry from the non-2.5 m data can be challenging, because SNe have SEDs that are quite different from stars. As a result, application of color terms derived from stars does not necessarily bring SN photometry onto the 2.5 m system. Clearly, the use of these data in conjunction with the 2.5 m photometry requires some understanding of the response differences between the telescopes and the SED of the SNe at different epochs (e.g., via the so-called *S*-corrections).

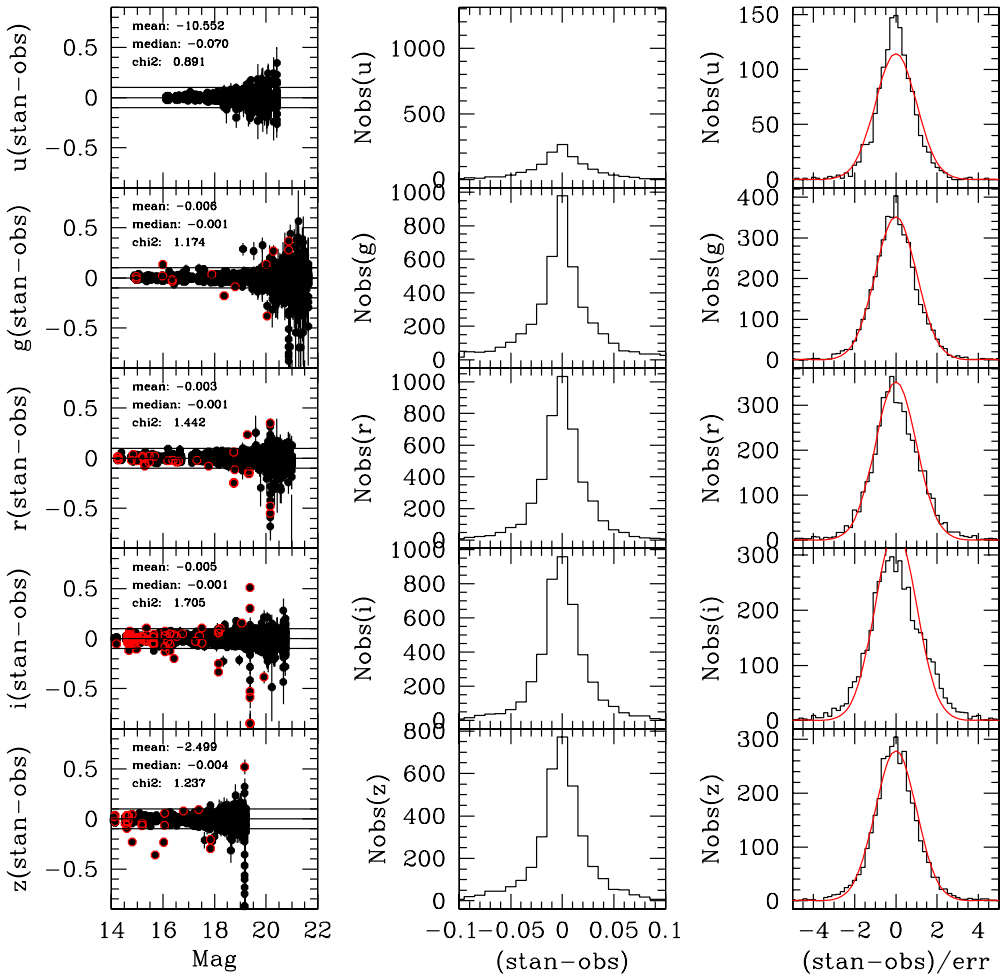

Figure 5. Photometry of stars near the 2005 SN, treating them as if they were SNe, allowing for an underlying background to be fit. The left panel shows the difference between the recovered magnitude and the known stellar magnitude as a function of magnitude. The central panel shows a histogram of error in the recovered magnitude, and the right panel gives a histogram of difference between recovered and calibration magnitudes, normalized by predicted photometric error. The curve in the right panel shows the expected Gaussian for the difference if the calculated errors are correct.

Unfortunately, it is usually rather difficult to get accurate measurements of the response functions of different systems. For some of the telescopes, we have obtained synthetic response functions from combinations of response functions of individual components. However, color terms computed from application of these response functions with libraries of stellar SEDs do not always match the measured color terms, suggesting errors in the response functions or the stellar libraries. This suggests that extreme caution should be used when applying products of individual component responses to determining transformations between observations using different photometric systems. We plan to investigate this in detail using measured response curves, the stellar calibration data, and several near-simultaneous observations of SNe by multiple telescopes.

Since the weather at APO was quite good for the 2005 season, the 2.5 m light curves provide good coverage even without the non-2.5 m data. Because of this and the complication of understanding the system responses of the non-2.5 m data, we have chosen not to include these data in our initial analyses and in the data release described in this paper. However, we hope to do so in the future, especially since we expect the other telescopes to contribute more in the last two observing seasons, mostly through followup of objects discovered late in the 2.5 m observing season; in 2005, many of the late objects do not have sufficient coverage to make them useful. It is in anticipation of using these data that we have included the discussion of the application of scene modeling to non-2.5 m data here.

5. PHOTOMETRY TESTS

We have performed a number of exercises to verify and improve the quality of the scene modeling photometry and error estimates. These tests also allow us to make educated decisions about what, if any, data cuts should be made before light-curve analysis.

5.1. Stellar Photometry

The first test treats real stars nearby the SNe as if they were SNe themselves, recovers light curves for them, and compares the derived brightnesses with the standard star catalog brightnesses. Using stars near the SN allows us to accurately understand how any errors in astrometry and the PSF are likely to affect the SN photometry. Unlike SNe, there is no galaxy background underneath these stars, but fitting for a model background that is zero is a valid, if somewhat unrealistic, test. In order to simulate an underlying zero galaxy background, we remove the star from the early epoch frames by replacing it with sky background taken from a nearby region of blank sky. The full stack of images (including the early epochs with the star removed and later epochs with the star retained) was then run

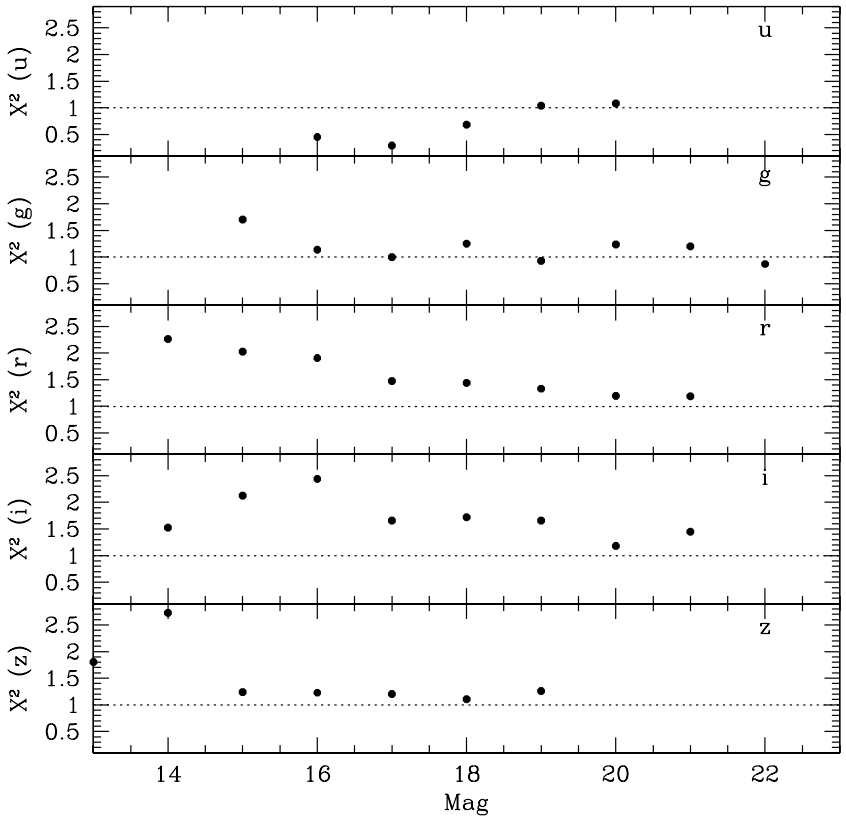

Figure 6. Reduced χ^2 for stars measured as if they were SNe, computed by comparing the individual recovered magnitude against their known magnitude. No sky error term has been included.

through the scene modeling software, allowing for a background to be fit.

Note, however, that the "known" calibration magnitudes (taken from Ivezic et al. 2007) are actually not *perfectly* known, and any errors in these will lead to increased scatter in our comparison (which includes many stars). To compensate for this, we have averaged all of our measurements of these stars (which make for many more measurements than what went into the Ivezic et al. 2007 catalog) and compare the individual measurements against this refined average.

Results are shown in Figure 5. The left panel plots the error in recovered brightnesses as a function of the stellar brightness. The central panel gives a histogram of the difference (standard − observed). In general, the recovered brightnesses are, to within estimated errors, consistent with the known brightness, with median errors from the entire sample of stars of only a few millimag.

The right panel shows the histogram of the difference normalized by the calculated error; if the error estimates were perfect, this should be a Gaussian of unit width. A more quantitative analysis of the error estimates is given in Figure 6, which shows the calculated reduced χ^2 from these distributions. For the brighter stars, the reduced χ^2 are near the expected value of unity for some filters, but they are a bit too large for other filters. We have investigated the source of this, and find that the larger χ^2 comes mostly from points with small predicted errors, less than 0.01 mag. This suggests that even with our procedure of adding a frame error, we still slightly underestimate our errors for the brightest sources. If we were to impose a 0.01 mag floor on the predicted errors, the χ^2 for the stars comes down near unity in most cases. We note that our SNe are essentially never so bright as to have such a small error. For the fainter stars, the χ^2 values are slightly too large in the *r* and *i* filters. This likely arises because no sky error has been included in these error estimates (see Section 5.3).

5.2. Pre-SNe Measurements

To test for errors in modeling a real underlying galaxy background, we measured the SNe flux for real SNe at epochs before the SN actually occurred, to see how well we would recover zero flux. Clearly, the galaxy model depends on the pre-SN epochs and the quality of that model will deteriorate if we remove too many of the pre-SN epochs from the list of images with constrained zero SNe flux. Because of this, we chose to do this test using the 2005 data, but looking at locations where SNe were discovered in 2006. This provides a good representation of the real situation for the 2005 SNe.

Figure 7 shows the results for measurements at the location of the 2006 SNe in the 2005 data. The ideal situation is to measure identically zero SN flux. The left panel shows the histogram of the difference between the observed and zero fluxes, in units of μJy (1 μJy $= 10^{-29}$ ergs cm^{-2} s^{-1} Hz^{-1}; a source with an apparent magnitude of 20 has a flux of 36.31 μJy). The right panel shows the histogram of the magnitude difference normalized by the predicted error. While there are a few points with measured brightness significantly different from zero, the bulk of the distribution follows the expected normal distribution. A more quantitative discussion of the estimated errors in presented in Section 5.3.

5.3. Artificial Supernovae

Finally, to test the accuracy of photometry at low flux levels against the galaxy background, we inserted artificial point

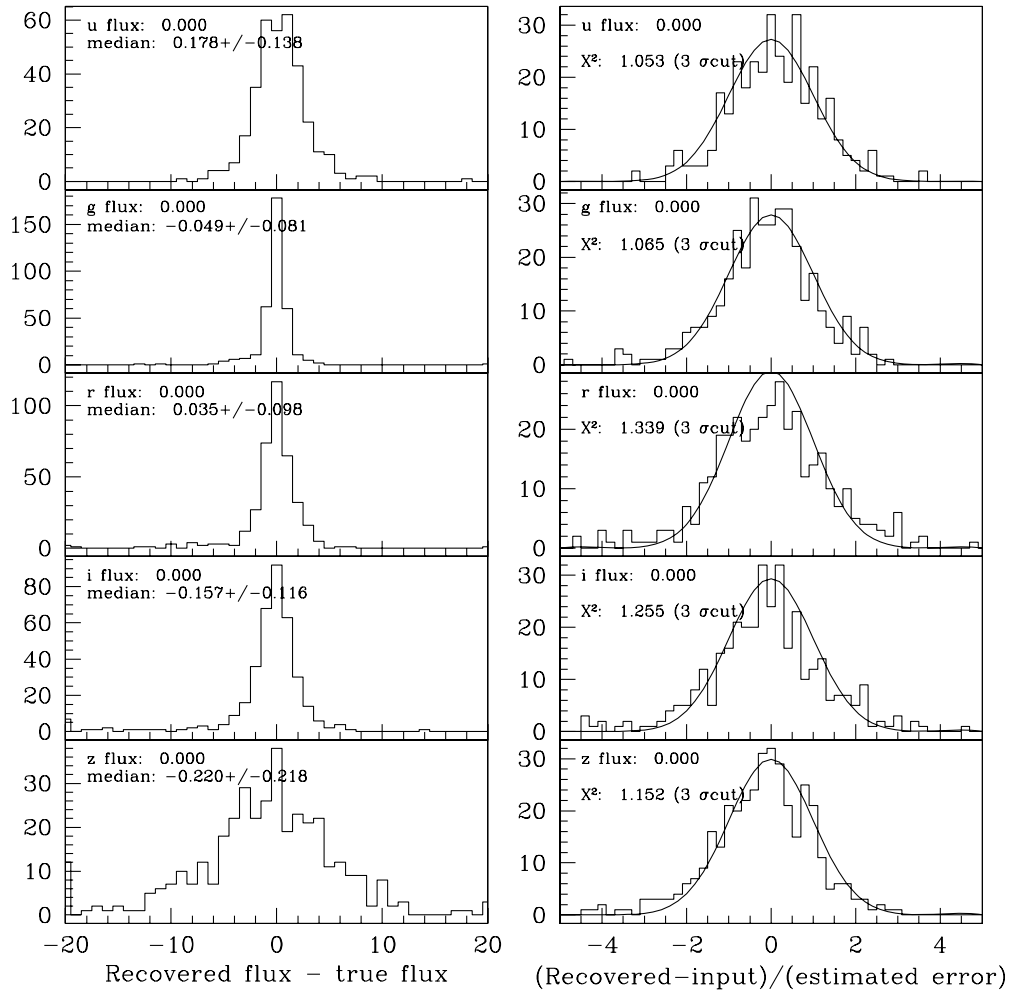

Figure 7. Photometry of 2005 epochs at the location of 2006 SNe, treating these as if they could have SN flux. The left panel shows the histogram of recovered fluxes, which should be zero; the units are μJy. The right panel shows a histogram of recovered flux normalized by predicted photometric error. The curve shows the ideal Gaussian of unit width.

sources into the frames and measured their brightnesses. Again, we used the locations of the 2006 SNe to place artificial sources into the 2005 frames. We inserted artificial SNe at 11 different flux levels. To reduce computation time, we split the 2006 sample of about 250 SNe locations into 11 groups, so at each level, we inserted artificial objects of about 22 different sky locations; at each location, artificial objects were placed in about 20 different epochs in the 2005 observations.

Artificial SN tests are not perfectly realistic because one must assume an astrometric solution, a photometric solution, and a PSF to insert the artificial objects, and usually the same quantities are used in the data reduction. For situations where uncertainties in any of these are the dominant source of error (bright objects), artificial SN tests are likely to provide overly optimistic results. As a result, we performed these tests only at a range of low flux levels. Artificial SNe were placed into the frames using the derived astrometric solution and photometric scalings, and the measured PSF. The entire stack of images was then run through the scene modeling software, and the measurements at the SN position were compared with the known artificial SNe brightnesses.

For each artificial SN test, we computed the median flux offsets between the measured and the input values, and calculate the mean fractional error of the recovered measurements. These are shown in the top panel of Figure 8 as a function of the input brightness. The error bars are the computed error of the median values, given the sample size. One can see that the flux is accurately recovered: to within a percent except for the faintest objects (and possibly even for these, given the statistical errors). The few points that deviate the farthest from a mean error of zero generally include locations where the artificial star was placed at a location with a bright galaxy background (i.e., in the center of a galaxy). It is clear that this is the most challenging situation for the accurate recovery of SN brightness; if the background is very bright, errors in the astrometry or PSF can throw off the recovered SN brightness.

Note that the error bars shown are the error of the sample mean; the statistical error on individual measurements is much larger than any small residual bias. This is demonstrated in the middle panel, which shows the mean of the error in recovered magnitude, normalized by the error estimate.

The bottom panel of Figure 8 shows a reduced χ^2 value, calculated from the square of the difference between recovered and input magnitudes, normalized by the estimated variance. If our error estimates are perfect, these should have values near unity. The open points show χ^2 as computed using the random error on the derived intensities; in general, these are slightly larger than unity. However, if one adds in quadrature the systematic errors from the sky determination (which should

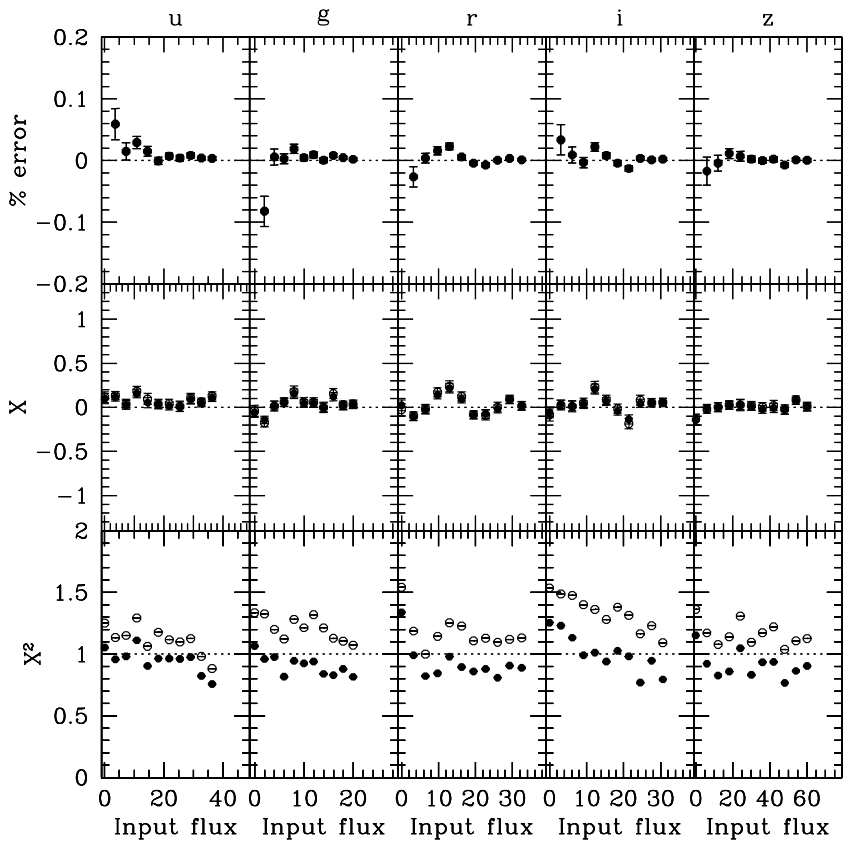

Figure 8. Mean recovered fluxes of artificial SNe at a range of different input fluxes; the units are μJy (note that $m = 20$ corresponds to 36.31 μJy). Each point represents an average of several hundred artificial objects placed in different 2005 epochs at the location of 2006 SNe positions. The top panels show the percent error of the recovered flux. The middle panels show the error in the derived brightness normalized by the predicted errors. The bottom panels show the χ^2 of the recovered brightnesses; open points show the values computed by using only the random error derived for the point source brightnesses, while the solid points include a term for errors in the sky level added in quadrature.

be random over a set of observations on different dates), then one gets the χ^2 values, which are shown with the filled points. These show that using an error estimate based on a combination of the flux-plus-sky error gives accurate error estimates, although our estimate of the sky error may be slightly too large.

6. LIGHT CURVES

In the 2005 SDSS SN season, 130 type Ia SNe were spectroscopically confirmed, along with additional 16 spectroscopically-probable Type Ia's. A complete list of all of the discovered SNe, along with positions and International Astronomical Union (IAU) designations, including non-Ia SNe, is presented in Sako et al. (2008).

We have used scene modeling to derive light curves for the 146 objects; the photometry data are available in the electronic version of this paper. Table 2 shows a portion of a sample data table for one of our SNe, SN2005hk, which has been discussed by Phillips et al. (2007). The files contain several lines of header information about the object: the SDSS internal candidate ID number, the IAU designation, the position, SDSS type, and redshift. In addition, approximate underlying galaxy surface brightnesses in each bandpass are given, as determined by the scene modeling photometry. The epoch of each observation is given as a modified heliocentric Julian date. The magnitudes in the file are given as asinh magnitudes (Lupton et al. 1999) on the native SDSS photometric system, using the softening parameters given in Stoughton et al. (2002). The fluxes are given in units of μJy, using the corrections to an AB system described in Section 3.1; by definition, an object with an AB magnitude of zero and a flat F_ν spectrum has a flux of $3.631 \times 10^9 \mu$Jy. Although no extinction correction has been applied to the measured brightnesses, the Galactic extinction, as estimated from the Schlegel et al. (1998) maps, is given in the file headers. The spectroscopic observations and the determination of the redshifts are described in Zheng et al. (2008). The redshifts, which were obtained by a variety of telescopes (Hobby-Eberly Telescope (HET), APO 3.5 m, Subaru Telescope, William Herschel Telescope, Nordic Optical Telescope, ESO New Technology Telescope, Wisconsin, Indiana, Yale, and NOAO (WIYN) Telescope, Keck Observatory, and the South African Large Telescope), are in the heliocentric frame.

In Figure 9, we show our derived light curves for the 146 SNe, sorted in order of redshift. These demonstrate the quality of the light curves. The plots include information about the IAU designation of these SNe and also give the estimated r-band galaxy surface brightness (from the scene modeling results) at the location of the SN.

7. CONCLUSION

We have presented a general technique, scene-modeling photometry, for extracting SNe photometry from multiple observations. A key feature of this technique is that it does not require resampling of data, resulting in accurate photometry and error estimates. Fitting all of the images as a sum of SN and galaxy light results in optimal use of all of the data, giving the highest

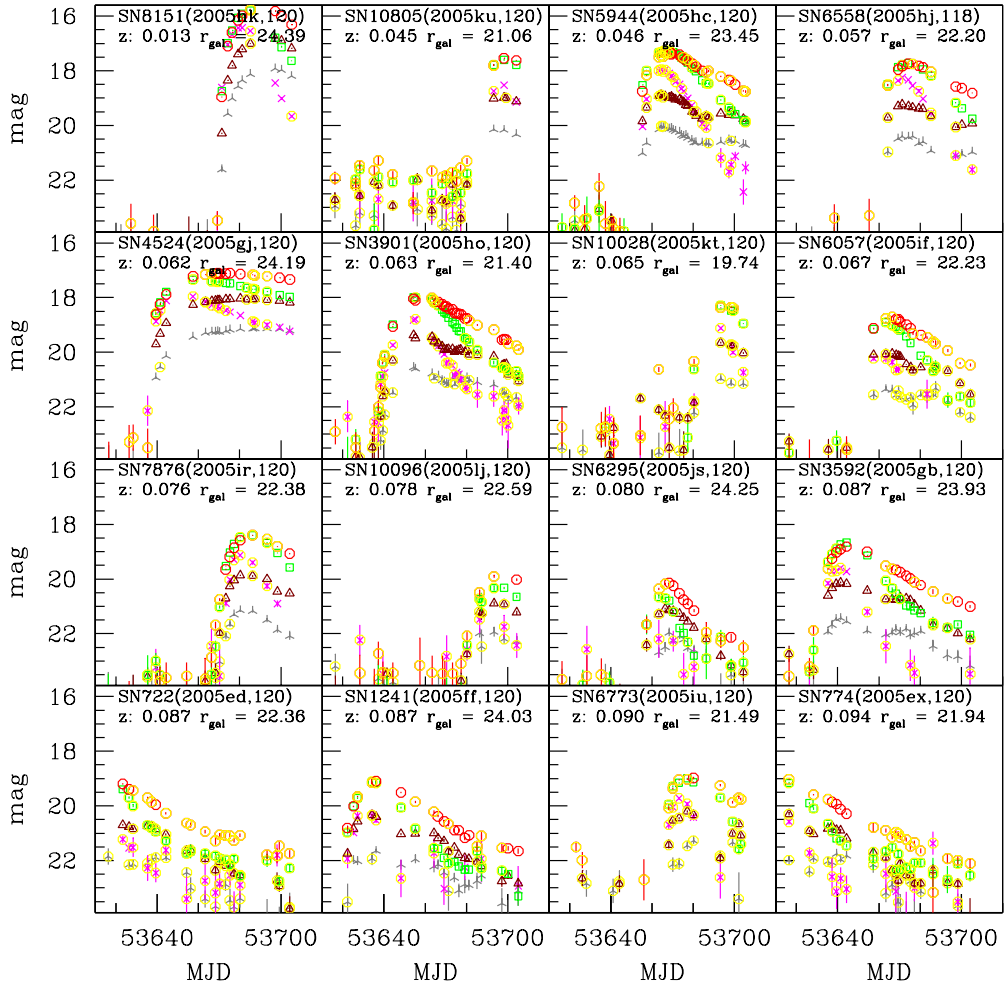

Figure 9. Derived light curves for the 2005 type Ia SNe, sorted by redshift. Red points are *r*, green points are *g*, magenta points are *u*, brown points are $i + 1$, and gray points are $z + 2$. Points circled in yellow have nonzero photometry flags; points with a flag value greater than 1024 (see text) are not plotted. The SDSS type is given, along with the IAU designation, in parentheses: type 120 is highly likely a type Ia SN confirmed by the SDSS survey team, type 119 objects are probably type Ia's, and type 118 is Ia's confirmed by another team.

(An extended version of this figure is available in the online journal.)

precision in the determination of the SN light curves. Another important consequence of this technique is that it is straightforward to combine data from several pointings or even telescopes, although the existence of nonzero color terms between different telescopes remains a limitation in the accuracy of the photometry.

We use the technique to extract photometry for all of the confirmed and probable type Ia SN candidates from the 2005 SDSS SN season. All of the data are accessible for public use via electronic tables (see Table 2) and will also be available through the SDSS SN Web site. These data provide the basis for the initial analysis of the SDSS SN survey.

Funding for the creation and distribution of the SDSS and SDSS-II has been provided by the Alfred P. Sloan Foundation, the Participating Institutions, the National Science Foundation, the U.S. Department of Energy, the National Aeronautics and Space Administration, the Japanese Monbukagakusho, the Max Planck Society, and the Higher Education Funding Council for England. The SDSS Web site is http://www.sdss.org/. This work is supported in part by a JSPS (Japan Society for the Promotion of Science) core-to-core program "International Research Network for Dark Energy" and by JSPS research grants. This work was also partially supported by Los Alamos National Laboratory University of California Directed Research and Development Fund. The HET is a joint project of the University of Texas at Austin, the Pennsylvania State University, Stanford University, Ludwig-Maximillians-Universität München, and Georg-August-Universität Göttingen; the HET is named in honor of its principal benefactors, William P. Hobby and Robert E. Eberly.

The SDSS is managed by the Astrophysical Research Consortium for the Participating Institutions. The Participating Institutions are the American Museum of Natural History, Astrophysical Institute Potsdam, University of Basel, Cambridge University, Case Western Reserve University, University of Chicago, Drexel University, Fermilab, the Institute for Advanced Study, the Japan Participation Group, Johns Hopkins University, the Joint Institute for Nuclear Astrophysics, the Kavli Institute for Particle Astrophysics and Cosmology, the Korean Scientist Group, the Chinese Academy of Sciences (LAMOST), Los Alamos National Laboratory, the Max-Planck-Institute for Astronomy (MPA), the Max-Planck-Institute for Astrophysics (MPiA), New

Table 2
Photometry for SN 2005hk (SDSS SN 8151)

FLAG[a]	MJD	FILT[b]	MAG[c]	MERR[d]	MSERR[e]	MGERR[f]	FLUX[g]	FLUXERR[h]	SERR[i]	GERR[j]	NPRE[k]	TELE	RUN[l]	STRIP[m]
0	53671.34315	1	18.745	0.012	0.001	0.001	1.128E+02	1.247E+00	1.479E-01	9.707E-02	10	sdss	5786	82S
0	53671.33983	2	18.960	0.018	0.005	0.001	9.419E+01	1.562E+00	4.341E-01	1.051E-01	12	sdss	5786	82S
0	53671.34066	3	19.288	0.023	0.003	0.002	6.880E+01	1.458E+00	2.055E-01	1.349E-01	12	sdss	5786	82S
0	53671.34232	4	19.609	0.096	0.066	0.012	5.115E+01	4.547E+00	3.125E+00	5.661E-01	12	sdss	5786	82S
0	53671.34149	0	18.612	0.035	0.003	0.003	1.349E+02	4.349E+00	3.877E-01	3.688E-01	10	sdss	5786	82S
0	53674.24276	1	16.989	0.012	0.000	0.000	5.686E+02	6.285E+00	1.035E-01	9.707E-02	10	sdss	5797	82S
0	53674.23944	2	17.103	0.006	0.000	0.000	5.210E+02	2.879E+00	1.724E-01	1.051E-01	12	sdss	5797	82S
0	53674.24027	3	17.352	0.009	0.001	0.000	4.093E+02	3.393E+00	4.193E-01	1.349E-01	12	sdss	5797	82S
0	53674.24193	4	17.576	0.017	0.004	0.002	3.336E+02	5.224E+00	1.132E+00	5.661E-01	12	sdss	5797	82S
0	53674.24110	0	17.044	0.023	0.001	0.001	5.718E+02	1.211E+01	2.840E-01	3.688E-01	10	sdss	5797	82S
0	53676.33207	1	16.523	0.004	0.000	0.000	8.734E+02	3.218E+00	7.615E-02	9.707E-02	10	sdss	5807	82S
0	53676.32875	2	16.598	0.004	0.000	0.000	8.295E+02	3.056E+00	7.532E-02	1.051E-01	12	sdss	5807	82S
0	53676.32958	3	16.811	0.005	0.001	0.000	6.736E+02	3.102E+00	3.147E-01	1.349E-01	12	sdss	5807	82S
0	53676.33124	4	17.016	0.010	0.003	0.001	5.587E+02	5.146E+00	1.419E+00	5.661E-01	12	sdss	5807	82S
0	53676.33041	0	16.675	0.014	0.001	0.000	8.032E+02	1.036E+01	3.986E-01	3.688E-01	10	sdss	5807	82S
...														

Notes. The online files include some additional ancillary information about each object, including the IAU designation, the coordinates, the redshift, the expected foreground extinctions from Schlegel et al. (1998), and the derived underlying galaxy brightnesses from the scene modeling.

[a] For details of (bitwise) values, see Section 4.1.1. A value of 0 indicates no lines, greater than 1024 is very likely a bad measurement, while a value between 0 and 1024 is likely okay but frame not used for the galaxy solution.

[b] 01234 = $ugriz$ bands.

[c] MAG is in the native SDSS photometric system, and is an asinh magnitude. No extinction correction has been applied.

[d] Random error in magnitude.

[e] Systematic magnitude error estimate from error in sky estimate.

[f] Systematic magnitude error estimate from error in underlying galaxy brightness.

[g] FLUX is in microJy using SDSS/AB correction (see text).

[h] Random error in flux.

[i] Systematic flux error estimate from error in sky estimate.

[j] Systematic flux error estimate from error in underlying galaxy brightness.

[k] RUN gives the SDSS run identifier.

[l] Strip gives the SDSS strip for this measurement.

[m] NPRE gives the number of pre-SN observations used.

Mexico State University, Ohio State University, University of Pittsburgh, University of Portsmouth, Princeton University, the United States Naval Observatory, and the University of Washington.

REFERENCES

Adelman-McCarthy, J., et al. 2008, ApJS, 175, 297
Astier, P., et al. 2006, A&A, 447, 31
Bohlin, R. C. 2000, AJ, 120, 437
Bohlin, R. C. 2007, in ASP Conf. Ser. 364, The Future of Photometric, Spectrophotometric, and Polarimetric Standardization, ed. C. Sterken (San Francisco, CA: ASP), 315
Bohlin, R. C., Dickinson, M. E., & Calzetti, D. 2001, AJ, 122, 2118
Frieman, J., et al. 2008, AJ, 135, 338
Fukugita, M., Ichikawa, T., Gunn, J. E., Doi, M., Shimasaku, K., & Schneider, D. P. 1996, AJ, 111, 1748
Gunn, J., et al. 1998, AJ, 116, 3040
Gunn, J. E., et al. 2006, AJ, 131, 2332
Hogg, D. W., Finkbeiner, D. P., Schlegel, D. J., & Gunn, J. E. 2001, AJ, 122, 2129
Ivezic, Z., et al. 2004, Astron. Nachr., 325, 583
Ivezic, Z., et al. 2007, ApJ, 134, 973
Kessler, R., et al. 2008, AJ submitted
Lupton, R. H., Gunn, J. E., & Szalay, A. S. 1999, AJ, 118, 1406
Oke, B. 1974, ApJS, 27, 21
Phillips, M. M., et al. 2007, PASP, 119, 360
Pier, J. R., Munn, J. A., Hindsley, R. B., Hennessy, G. S., Kent, S. M., Lupton, R. H., & Ivezic, Z. 2003, AJ, 125, 1559
Sako, M., et al. 2008, AJ, 135, 348
Schechter, P. L., Mateo, M., & Saha, A. 1993, PASP, 105, 1342
Schlegel, D., Finkbeiner, D., & Davis, M. 1998, ApJ, 500, 525
Smith, J. A., et al. 2002, AJ, 123, 2121
Stetson, P. B. 1987, PASP, 99, 191
Stoughton, C., et al. 2002, AJ, 123, 485 (Early Data Release)
Tucker, D., et al. 2006, Astron. Nachr., 327, 821
York, D. G., et al. 2000, AJ, 120, 1579
Zheng, C., et al. 2008, AJ, 135, 1766